PHYSICAL REVIEW D **77,** 044011 (2008)

Measuring eccentricity in binary black-hole initial data

Jason D. Grigsby* and Gregory B. Cook†

Department of Physics, Wake Forest University, Winston-Salem, North Carolina 27109, USA

(Received 28 June 2007; published 8 February 2008)

Initial data for evolving black-hole binaries can be constructed via many techniques, and can represent a wide range of physical scenarios. However, because of the way that different schemes parametrize the physical aspects of a configuration, it is not always clear what a given set of initial data actually represents. This is especially important for quasiequilibrium data constructed using the conformal thin-sandwich approach. Most initial-data studies have focused on identifying data sets that represent binaries in quasicircular orbits. In this paper, we consider initial-data sets representing equal-mass black-hole binaries in eccentric orbits. We will show that effective-potential techniques can be used to calibrate initial data for black-hole binaries in eccentric orbits. We will also examine several different approaches, including post-Newtonian diagnostics, for measuring the eccentricity of an orbit. Finally, we propose the use of the ''Komar-mass difference'' as a useful, invariant means of parametrizing the eccentricity of relativistic orbits.

DOI: 10.1103/PhysRevD.77.044011 PACS numbers: 04.20.−q, 04.25.dg, 04.70.Bw, 97.80.−d

I. INTRODUCTION

The possible detection of gravitational waves by detectors such as LIGO and LISA is driving rapid progress in the binary black-hole (BBH) problem. The final stages of the inspiral and coalescence are believed to be primary sources of gravitational waves at frequencies accessible by such detectors. Theoretical models that accurately predict these final stages of inspiral are needed to help analyze and improve the rate of detection with future data. There are two techniques commonly used to study such systems, the post-Newtonian (PN) approximation and numerical relativity (NR). A detailed comparison has recently been carried out between high accuracy NR simulations and a set of PN approximants for the gravitational waves produced by nonspinning equal-mass black holes on a quasicircular adiabatic inspiral [1]. This study clearly shows the excellent agreement between NR and PN methods as well as the expected increasing level of uncertainty in the PN approximations as the binary separation becomes small.

Numerical relativity breaks any simulation into two parts, the specification of initial data and the numerical time evolutions of this data. With recent advances in evolutions [2–10], it is as important as ever to fully understand the initial data each simulation is starting with. It is well known that BBHs starting with large separation will evolve toward an adiabatic inspiral that follows a series of quasicircular orbits [11]. Most numerical work to date in both the construction of BBH initial data and evolutions has focused on quasicircular configurations. But the study of binaries in truly eccentric orbits near coalescence may be important for gravity-wave detectors (especially LISA) and, in any case, is of considerable theoretical interest.

*grigjd3@wfu.edu
†cookgb@wfu.edu

To predict which initial-data sets will yield binaries in quasicircular orbits, two techniques have commonly been used, one based on an effective-potential (EP) method [12] and the other on the Komar-mass ansatz [13]. The two methods have been contrasted and largely agree, with significant differences occurring only at small BBH separations [14,15]. For initial-data schemes where the linear momenta of the individual black holes in a binary can be directly specified [16,17], appropriate values for the momenta to yield circular orbits can also be obtained from PN results [7,18].

When the momenta of the black holes are specified directly, the path to obtain elliptical orbits seems straightforward: simply increase or decrease the momenta of each hole from its value for a quasicircular orbit. However, when quasiequilibrium methods are used to construct the initial data, noncircular orbits clearly break the notion of quasiequilibrium since the black holes will no longer remain stationary in a corotating frame. A primary goal of this paper is to examine how current quasiequilibrium methods for constructing BBH initial data can be extended to construct general eccentric configurations.

We begin in Sec. II with an overview of the quasiequilibrium method we use to construct BBH initial data, emphasizing the aspects that will be most relevant to our subsequent discussion. In Sec. III, we will discuss various aspects of effective potentials in the context of their use with BBH initial data. In particular, we will justify as fully as we can the extension of these effective potentials to BBHs in eccentric orbits. In Sec. IV we will explore and compare several definitions of eccentricity, and will motivate the use of the ''Komar-mass difference'' as an invariant means of parametrizing BBHs in eccentric orbits. All of the preceding discussions have dealt with nonspinning black holes. In Sec. V, we will briefly discuss the case of corotating black holes. We end the paper in Sec. VI with some conclusions.

II. INITIAL DATA

The binary black-hole initial-data sets that are used below were described in detail in Refs. [14,19] and references within. Here, we give an overview of the methods used to construct the initial data, elaborating only on the details most relevant to finding black-hole binaries in quasicircular orbits.

Our initial-data sets were constructed within the *extended conformal thin-sandwich* (CTS) approach [20,21]. This approach is based on the standard 3 + 1 decomposition where the space-time interval is written as

$$ds^2 = -\alpha^2 dt^2 + \gamma_{ij}(dx^i + \beta^i dt)(dx^j + \beta^j dt). \quad (1)$$

Here, γ_{ij} is the spatial metric, and α and β^i are the lapse function and shift vector. Minimal initial data for a Cauchy evolution requires that we fully specify γ_{ij} and the extrinsic curvature K_{ij} (essentially a first time derivative of the spatial metric) defined as

$$K_{ij} \equiv -\tfrac{1}{2}\mathcal{L}_n \gamma_{ij}, \quad (2)$$

where n^μ is the timelike unit normal to the $t = \text{const}$ initial-data surface.

The CTS approach requires a conformal decomposition of γ_{ij}, and that we specify the conformally related metric $\tilde{\gamma}_{ij}$. In this work we have taken $\tilde{\gamma}_{ij}$ to be flat. The time derivative of the conformal metric $\partial_t \tilde{\gamma}_{ij}$ must also be specified, along with the trace of the extrinsic curvature K. We fixed both quantities to be zero. The CTS approach then requires that we determine the conformal factor ψ relating γ_{ij} and the conformal metric, and the shift vector β^i. These are obtained by solving elliptic versions of the Hamiltonian and momentum constraint equations (see Ref. [14] for details). Finally, the extended CTS approach also requires that we determine the lapse function α by fixing the time derivative of the trace of the extrinsic curvature and then solving the evolution equation for the trace of the extrinsic curvature as an elliptic equation. We fixed the trace of the extrinsic curvature to be constant in time, $\partial_t K = 0$.

In constructing the initial data, we excised the black-hole interior from the computational domain, requiring us to impose boundary conditions at these excision surfaces when solving the elliptic equations for ψ, β^i, and α. We demanded that each black hole be in quasiequilibrium by imposing the boundary conditions worked out in Refs. [19,22]. The assumptions of quasiequilibrium are essentially the same as those required of an "isolated horizon" (see Refs. [23–25]). We must also impose boundary conditions at the outer boundary of the computational domain (either at infinity or some large radial distance from the black holes). For this, we assume that our configuration is asymptotically flat. However, asymptotic flatness does not fully fix the boundary conditions on the constrained data. The asymptotic condition on the shift is

$$\beta^i|_{r\to\infty} = (\mathbf{\Omega}_0 \times \mathbf{r})^i, \quad (3)$$

where $\mathbf{\Omega}_0$ is an angular velocity vector.

The time coordinate threading through our initial-data slice is defined by

$$t^\mu \equiv \alpha n^\mu + \beta^\mu. \quad (4)$$

Imposing Eq. (3), we see that $\mathbf{\Omega}_0$ determines the rotation of the "helical" time coordinate. If a binary system were in true equilibrium, the time coordinate would generate a symmetry and the bodies would move in circular orbits along integral lines of the time coordinate. For relativistic systems, the binary can at best be only in quasiequilibrium and the time coordinate generates an approximate symmetry. Nevertheless, $\mathbf{\Omega}_0$ represents the orbital angular velocity of the binary as measured by observers at infinity. From a computational perspective, $\mathbf{\Omega}_0$ must be chosen. *Ultimately, it is the effect of different choices for* $\mathbf{\Omega}_0$ *that we will be exploring in this paper.*

In Ref. [14], two independent methods for choosing the magnitude of $\mathbf{\Omega}_0$ were compared. Both methods attempt to produce a binary system that is in quasiequilibrium with the black holes in quasicircular orbits. One method is based on the Komar-mass ansatz, first proposed by Gourgoulhon *et al.* [13], which posits that if Ω_0 is chosen so that the Arnowitt-Deser-Misner (ADM) energy $E_{\rm ADM}$ and the Komar mass $M_{\rm K}$ of a system are equal, then the system will be nearly stationary (i.e., in quasiequilibrium) and the binary will be in a quasicircular orbit. These masses are defined via

$$E_{\rm ADM} = \frac{1}{16\pi}\oint_\infty \nabla_j(\mathcal{G}^j_i - \delta^j_i \mathcal{G}) d^2S^i, \quad (5)$$

$$M_{\rm K} = \frac{1}{4\pi}\oint_\infty (\nabla_i \alpha - \beta^j K_{ij}) d^2S^i, \quad (6)$$

where $\mathcal{G}_{ij} \equiv \gamma_{ij} - f_{ij}$, f_{ij} is the flat metric, and ∇_j is the covariant derivative compatible with γ_{ij}. The second method assumes that quasicircular orbits are found at the minima of a reduced two-body effective potential. Effective potentials will be described in more detail in Sec. III.

In Ref. [14], we showed that the circular-orbit configurations produced by both methods agree remarkably well for both nonspinning and corotating black-hole binaries. Here, we simply show a figure that directly compares sets of circular-orbit models as we vary the binary separation. Figure 1 displays the EP curves for nonspinning equal-mass black-hole binaries as computed in Ref. [14]. The vertical axis displays the dimensionless binding energy of the binary $E_{\rm b}/\mu$, where $E_{\rm b}$ is defined in Eq. (7), $\mu \equiv m_1 m_2/m$ is the reduced mass of the system and $m \equiv m_1 + m_2$ is the total mass of the binary. The horizontal axis displays the dimensionless proper separation of the binary ℓ/m. It is important to note that each EP curve consists of a

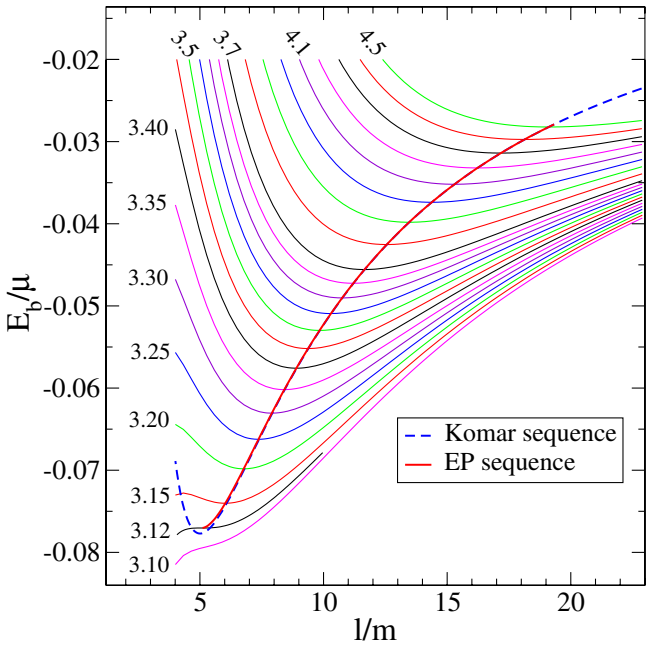

FIG. 1 (color online). Effective-potential plot for nonspinning equal-mass black holes constructed from numerical initial data [14]. The thin solid (multicolor) lines are individual EP curves. Some of these EP curves are labeled by their value of $J/\mu m$. Passing through the local minima of these EP curves and drawn as a bold (red) line is the EP sequence of quasicircular orbits. The Komar sequence of quasicircular orbits is displayed as a dashed (blue) line.

sequence of models where the value of Ω_0 changes monotonically. Passing through the minima of the EP curves is the ''EP sequence'' defined as the sequence of quasicircular orbit models where quasicircular orbits are defined via the effective-potential method. Also shown in Fig. 1 is the ''Komar sequence'' defined as the sequence of quasicircular orbit models defined via the Komar-mass ansatz. It is clear that the two sequences agree quite well except for the smallest separations. See Ref. [14] for a more detailed comparison. Most important for our considerations is that both the Komar-mass and EP methods choose particular models on each EP curve, with very similar values of Ω_0, as quasicircular orbit models.

When the CTS equations and excision boundary conditions as described above are used to construct initial data for binaries in quasicircular orbit, the resulting data are consistent with a system in quasiequilibrium. In particular, we expect both bodies in the binary to be following the integral curves of an approximate helical Killing vector (the time coordinate). Furthermore, half of the initial data that must be specified is also consistent with this notion of quasiequilibrium. Recall that the conformal metric $\tilde{\gamma}_{ij}$, the trace of the extrinsic curvature K, and their time derivatives must be specified, and that *we take all of the time derivatives to vanish*. As long as the binary is in a circular orbit, the notion of quasiequilibrium is satisfied.

We are left to wonder, though, what does the initial data represent if we choose Ω_0 so that the binary is *not* in a quasicircular orbit? We are forced to give up the notion that the helical time vector represents an approximate Killing vector of the space-time. In Ref. [14], we made the assertion that the resulting initial data would represent a binary at either pericenter or apocenter of a general bound or unbound orbit. This assertion is grounded in the hypothesis that setting $\partial_t \tilde{\gamma}_{ij} = 0$ is sufficient to set the initial radial velocity of the black holes to zero. Our goal below is to see if this generalized interpretation of the initial data is reasonable.

III. EFFECTIVE POTENTIALS

In Newtonian physics, 1D effective potentials nicely capture the important features of certain dynamical systems. In the case of the reduced gravitational 2-body problem, for a given orbital angular momentum, the effective potential can be used to locate the turning points for an elliptic orbit of given energy, or the radius and energy of a circular orbit. No exact 1D effective potential can be rigorously and uniquely derived for the fully relativistic gravitational 2-body problem, although useful effective potentials can be defined within any PN approximation. Within the fully relativistic theory, a useful effective potential has been defined [12,15,26,27] in direct analogy with the Newtonian gravitational effective potential.

In essence, an EP curve is the total energy of the system measured along a sequence of configurations where the radial separation varies, while all other physical parameters are held fixed. In order to correspond to an effective potential, the velocity of the generalized coordinate that is allowed to vary (the radial separation in this case) must vanish so that there is no associated (radial) kinetic energy. Binary systems in bound orbits with vanishing radial velocity are either at apocenter or pericenter, and collectively we refer to these as turning points in the orbit. Also, in order for the concept of an effective potential to be applicable, it must be true that the dissipative effects of radiation reaction must occur on a time scale that is much larger than an orbital period. Clearly, this approximation will break down for binaries that reach sufficiently small separations.

For black-hole binaries, we define each EP curve used in this work as a sequence of initial-data configurations where the apparent-horizon masses of the individual black holes (m_1 and m_2), the magnitude and direction of the spins of the individual black holes, and the total angular momentum of the system are held constant. We also require that the binary be at a turning point in the orbit. The value of the effective potential at each point on the EP curve is taken to be the binding energy:

$$E_b \equiv E_{\mathrm{ADM}} - m_1 - m_2. \tag{7}$$

We emphasize that there are several ''uncertainties'' within this definition which necessarily lead to some level of

uncertainty in any results that are based on it. These uncertainties stem from the fact that there is no unique way to define the total mass, spin, or linear momentum for an individual black hole in a binary system. When needed, we define the total mass of a black hole using the Christodoulou formula [28]

$$M^2 = M_{\rm irr}^2 + \frac{S^2}{4M_{\rm irr}^2}, \tag{8}$$

where the irreducible mass $M_{\rm irr}$ is approximated by the apparent-horizon mass $m_{1,2}$ and the spin S is computed via some quasilocal approximation (cf. Refs. [14,29]).

Of more immediate concern is the fact that we cannot uniquely define the linear momentum of each hole. As with spin, a quasilocal linear momentum can be defined (cf. Ref. [30]). We have examined this, but the radial component of the momentum, though small, does not vanish even for quasicircular orbits. Instead of trying to directly measure the radial velocity (or momentum) to determine if a given initial-data set is at a turning point, we will compare our numerical EP curves against PN results.

There are at least two approaches for considering eccentric binaries within the PN framework (cf. Ref. [31] and references within). In this work, we fill follow the approach of Mora and Will [32] who introduced third-order conservative post-Newtonian equations for the energy and angular momentum of a system in terms of a single eccentricity ϵ and its associated inverse semilatus rectum ζ. In that work, the authors treated the black holes as having zero spin and ignored dissipative terms. One can find the orbital angular velocity at either pericenter or apocenter through the authors' choice of definition of ϵ and ζ used in creating these equations. In order to include the spin of the black holes, and to parametrize the equations in terms of irreducible mass instead of total masses, it becomes necessary to include correction terms that create equations of the following form:

$$E(\epsilon, \zeta, \omega) = E_{\rm ADM}(\epsilon, \zeta) + E_{\rm self}(\epsilon, \zeta, \omega) + E_{\rm N,corr}(\epsilon, \zeta, \omega) + E_{\rm spin}(\epsilon, \zeta, \omega), \tag{9}$$

$$J(\epsilon, \zeta, \omega) = J_{\rm ADM}(\epsilon, \zeta) + S(\epsilon, \zeta, \omega) + J_{\rm N,corr}(\epsilon, \zeta, \omega) + J_{\rm spin}(\epsilon, \zeta, \omega). \tag{10}$$

In these equations ω represents the spin angular velocities of the black holes.[1] The self-energy and spin terms ($E_{\rm self}$ and S) are derived as expansions of the Kerr formulas relating mass, spin, and rotational angular velocity. The Newtonian correction terms ($E_{\rm N,corr}$ and $J_{\rm N,corr}$) stem from the conversion of total mass to irreducible mass and the "spin" terms ($E_{\rm spin}$ and $J_{\rm spin}$) represent spin-orbit effects.

[1]We use a single parameter ω for simplicity. In general, specifying the spin of two black holes would require six parameters.

The parameter space of these equations, for the case of nonspinning holes, can be seen in Figs. 5 and 6 which will be discussed later.

With this parametrization, one can easily construct 3PN EP curves. In Fig. 2, we plot for comparison the EP curves for nonspinning, equal-mass binaries from both the numerical data and the 3PN equations. The energy is plotted as a function of the dimensionless orbital angular velocity $m\Omega$, where small $m\Omega$ corresponds to large orbital separation. Included on the graph is data from the Komar sequence and the EP sequences extracted from the minima of the 3PN EP curves and the numerical EP curves.

At large values of angular momentum (large orbital separation), the solid 3PN data curves agree well with the dashed numerical data curves. The numerical data and the 3PN data begin to diverge as the angular momentum decreases. This is not surprising as it is well known that both numerical quasiequilibrium models and the PN expansion become less accurate for tighter binary systems. It seems from the good agreement between numerical and 3PN EP curves that the numerical data we construct using the CTS approach are reasonably close to turning points, and clearly asymptote to turning points as the system becomes more Newtonian.

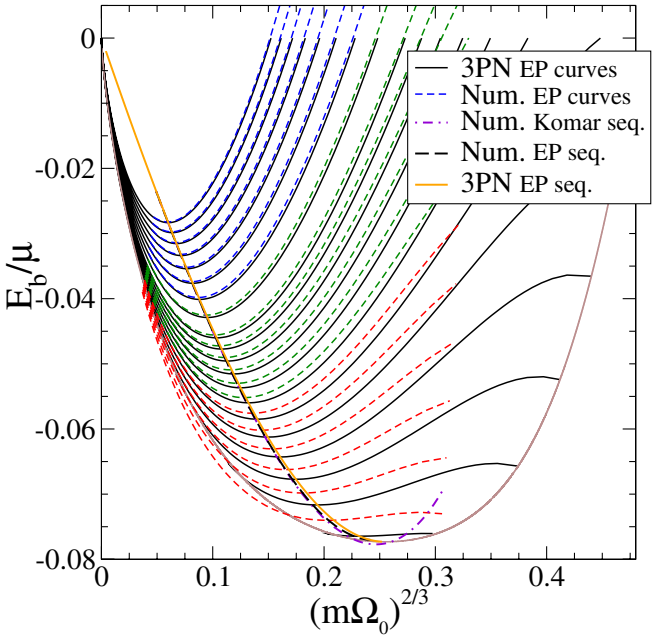

FIG. 2 (color online). EP curves for nonspinning equal-mass black holes from both numerical and 3PN data. Numerical EP curves are plotted as short-dashed (blue, green, and red) lines. 3PN EP curves are plotted as solid (black) lines. The Komar sequence through the numerical data is plotted as a dash-dotted (purple) line. The EP sequence through the numerical data is plotted as a long-dashed (black) line. The EP sequence through the minima of the 3PN data is plotted as a light-solid (orange) line. A boundary of the allowable region for 3PN equations is shown as a light-solid (brown) line at the ends of the 3PN curves.

IV. MEASURING ECCENTRICITY

The comparison of the numerical EP to the 3PN EP curves in Sec. III gives us confidence that the numerical data represent systems at either pericenter or apocenter. Since each numerical EP curve is constructed from a sequence of models where the mass, angular momentum, and spins are held constant and are at turning points, it is reasonable to use these curves as one method of defining the eccentricity for a given model.

For Newtonian binaries, eccentricity can be measured using relative separation at pericenter d_p and apocenter d_a:

$$\epsilon_d \equiv \frac{d_a - d_p}{d_a + d_p}. \tag{11}$$

We use ϵ_d to denote the eccentricity of numerical models based on coordinate separations. By applying Newtonian equations of motion, one can replace the above definition of eccentricity parametrized by relative separation with a version that depends on the orbital angular velocities at pericenter Ω_p and apocenter Ω_a. Not only is the eccentricity found in those terms, but the dimensionless inverse semilatus rectum can also be found using the same parameters [32].

$$\epsilon_\Omega \equiv \frac{\Omega_p - \Omega_a}{\Omega_p + \Omega_a}, \tag{12}$$

$$\zeta \equiv \left(\frac{\sqrt{m\Omega_p} + \sqrt{m\Omega_a}}{2}\right)^{4/3}. \tag{13}$$

We use ϵ_Ω to denote the eccentricity of our numerical models as measured using orbital angular velocities. The following relationships follow directly from these equations:

$$\zeta = \left(\frac{m\Omega_p}{(1+\epsilon_\Omega)^2}\right)^{2/3} = \left(\frac{m\Omega_a}{(1-\epsilon_\Omega)^2}\right)^{2/3}. \tag{14}$$

We note that these equations (at either pericenter or apocenter) are the only places in any of our work where the sign of the eccentricity matters, and so for the remainder of the paper we will ignore the middle (pericenter) relationship and *assume eccentricity is negative at pericenter*. This has the added benefit of simplifying many of the figures below.

A. Direct measurement

Our next goal is to determine if the definition of eccentricity in Eq. (12) yields reasonable results. We start by computing ϵ_Ω for the nonspinning equal-mass models represented in the numerical EP curves displayed in Fig. 2 (also seen in Fig. 1). The measured eccentricities are shown in Fig. 3, plotted against $m\Omega$. The ϵ_Ω definition of eccentricity should give reasonable results when the corresponding orbit is sufficiently Newtonian. The orbits become more relativistic as the total angular momentum

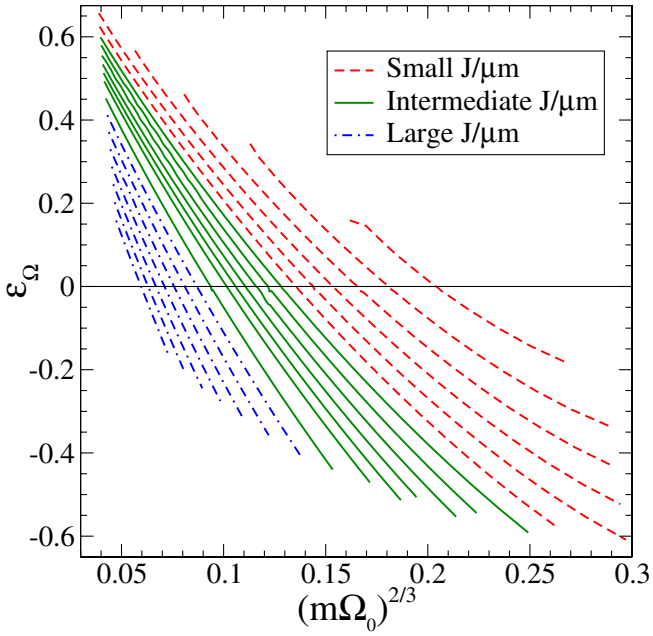

FIG. 3 (color online). Eccentricity of nonspinning equal-mass black holes computed along numerical EP curves. The ϵ_Ω definition of eccentricity is plotted against the orbital angular velocity. Negative values of ϵ_Ω correspond to models at pericenter, while positive values correspond to apocenter. Large values of the orbital angular momentum are plotted as dot-dashed (blue) lines, intermediate values as solid (green) lines, and small values as dashed (red) lines.

associated with the orbit gets smaller. Throughout this paper, we will use the following convention to easily differentiate which EP curves represent large, intermediate, and small values of angular momentum. EP curves with dot-dashed lines represent large values of angular momentum, solid lines denote the middle range of angular momentum, and the dashed lines have small values of angular momentum.

Figure 3 shows only a limited range of eccentricities for each value of angular momentum. There are several reasons for this, both physical and computational. First, to compute the eccentricity, we require data from two corresponding turning points on the same EP curve. That is, we need two points with the same value of the binding energy. Because we do not construct models at arbitrarily large separation, some data at pericenter have no matching data at apocenter. In this case, the eccentricity cannot be computed. Clearly, we cannot compute eccentricities using this method for pericenter data corresponding to unbound orbits, but there are additional limitations associated with the shape of the effective potential at small separation. Because of strong-field effects, the effective potentials reach a local maximum at small separation (cf. the effective potential for massive test particles orbiting Schwarzschild). For bound orbits, we are limited to computing eccentricities for configurations with energies lower

than that of the local maximum for each EP curve. So, the eccentricities plotted in Fig. 3 correspond to data in the neighborhood of the local minimum of each EP curve and extending only as far as the lowest local maximum on either side.

To test whether the numerical data is behaving as expected, we turn to the definition of eccentricity found in ϵ_d. This definition should be reasonable for large separations, but will break down as the coordinate separation of the two black holes decreases because of coordinate effects near the black holes. In Fig. 4, we show the relative difference of the two measurements $(\epsilon_\Omega - \epsilon_d)/\epsilon_\Omega$. Note that we have manually removed data corresponding to points near the minima of the EP curves since both definitions of eccentricity yield zero at the minimum and the relative error for neighboring points is dominated by numerical noise. However, it is easy to find where those points would have been as the different lines become somewhat jagged in the region of zero eccentricity. This is a good example of how definitions of eccentricity for strong field binaries are not unique.

Figure 4 shows the expected behavior. For large separations (large $J/\mu m$) the coordinate separation d and the orbital angular velocity should both yield reasonable estimates of the eccentricity and we see that the relative error is tending to zero as $J/\mu m$ increases. Clearly, the gauge dependence of the coordinate separation d will cause ϵ_d to become less reliable for smaller separations (small $J/\mu m$), and indeed we see the relative difference increase as $J/\mu m$ decreases. Because the orbital angular velocity Ω_0 is gauge

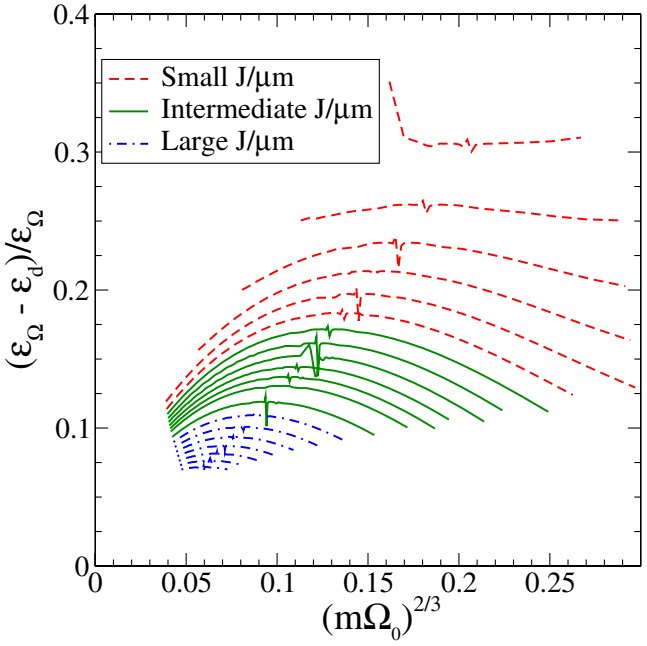

FIG. 4 (color online). The relative difference between the ϵ_Ω and ϵ_d definitions of eccentricity for the nonspinning equal-mass black-hole numerical EP curves. Lines as in Fig. 3.

independent, we expect that ϵ_Ω will yield a better definition of the eccentricity; however, we need an independent standard against which we can measure the reliability of ϵ_Ω.

B. Post-Newtonian measurement

To test ϵ_Ω in the more relativistic regime we return to post-Newtonian theory. The 3PN equations for the energy and angular momentum in Eqs. (9) and (10) can be used to compute the eccentricity of initial data in several ways, all using information from a single initial-data configuration [32–34]. The two most useful ways are based on using values for either E_b and Ω_0 or J and Ω_0 from a given initial-data set. Both methods yield similar but distinct values for the eccentricity. We will denote eccentricities obtained using the energy via ϵ_{E_b}, and using the angular momentum via ϵ_J.

To use Eqs. (9) and (10) to find eccentricity, we need to simplify the dependencies. Those equations depend on the eccentricity ϵ, the inverse semilatus rectum ζ, and the individual black-hole spins (represented by ω). The spin dependence can always be fixed. For now, we consider nonspinning black holes. Next we apply Eq. (14) to replace ϵ with $m\Omega$ and ζ. The equations now depend on only $m\Omega$ and ζ. To find a 3PN value of ζ, we set one of the equations (say the energy equation) to the constant (energy) taken from an initial-data set and replace $m\Omega$ with its value from

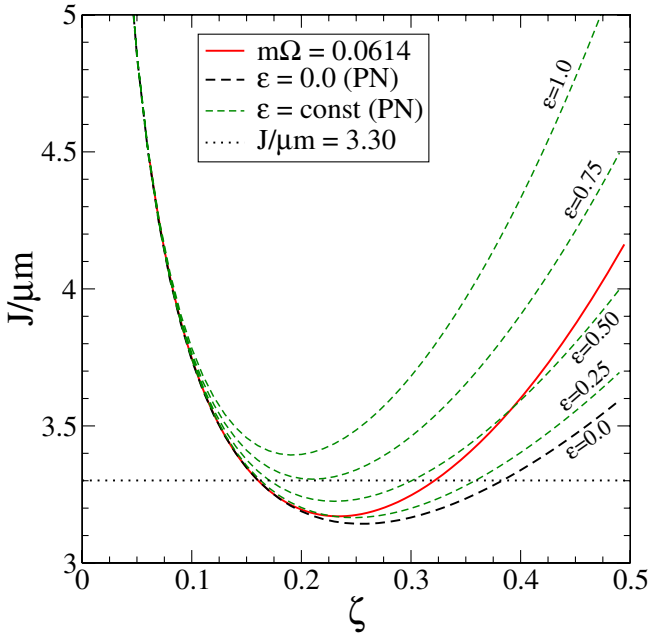

FIG. 5 (color online). Parameter space of $J(\epsilon, \zeta)$ [Eq. (10)] for nonspinning equal-mass black holes. Short-dashed (green or black) lines of constant ϵ are constructed using the 3PN equations. The solid (red) line represents all 3PN models with a specific value of $m\Omega = 0.0614$ corresponding to a particular numerical model. The horizontal dotted (black) line represents the corresponding orbital angular momentum of that model.

the same data set. We can then use one-dimensional root finding to obtain a value for ζ. Finally, using Eq. (14) again, we can obtain ϵ.

There is an issue when using root-finding methods on the modified equations. Equations (9) and (10) are polynomials with multiple roots, so we must determine which value of ζ to use. Figure 5 shows the parameter space for the 3PN angular momentum from Eq. (10) for the case of nonspinning equal-mass black holes. The angular momenta for lines of constant eccentricity are plotted against ζ as dashed lines. A solid line shows all 3PN configurations having a constant value of $m\Omega = 0.061\,355$. This value of $m\Omega$ was chosen because it corresponds to the minimum of one of the numerical EP curves. The horizontal dotted line displays the angular momentum from that EP curve. As can be seen, there are two values of ζ where these two lines intersect, and both correspond to valid roots of the equation. The smallest positive root corresponds to a very small eccentricity which we would expect for the given data set. The second smallest positive root yields an eccentricity somewhere between $\epsilon_J = 0.25$ and $\epsilon_J = 0.50$. It is unlikely that the minimum of an EP curve would have such high eccentricities and negative values of ζ are not allowed, so we always choose the smallest positive root for ζ. The 3PN energy from Eq. (9) yields similar results as can be seen in Fig. 6. Again, we always choose the smallest positive root for ζ.

In Fig. 7 we show the eccentricity ϵ_{E_b} of the same EP curves considered in Fig. 3 but computed using the 3PN energy equation. The minima of the EP curves, which would have $\epsilon_\Omega = 0$, are marked with $\times$'s. Qualitatively, these results resemble the previous direct measurements shown in Fig. 3; however, there are differences. First, note that the minima of the EP curves do not correspond exactly to $\epsilon_{E_b} = 0$ (as first noticed in Refs. [32–34]). Also, for large values of $J/\mu m$, ϵ_{E_b} can be evaluated for more of the data points on these EP curves than is possible for ϵ_Ω. The evaluation of ϵ_Ω was limited in this range because the numerical data did not extend out to sufficiently large separations and ϵ_Ω requires pairs of turning points to measure the eccentricity. Because ϵ_{E_b} requires information from only a single initial-data set, it can be computed for some data points where ϵ_Ω cannot. While not presented here, using the angular momentum equation to compute ϵ_J delivers results that are qualitatively similar.

Finally, our goal has been to gauge whether or not ϵ_Ω was a reasonable definition of eccentricity. In Fig. 8, we show the difference between the ϵ_Ω and the 3PN definition of eccentricity ϵ_{E_b}. We plot $\epsilon_\Omega - \epsilon_{E_b}$ against ϵ_Ω rather than a relative difference to avoid division by small number issues that make the graph difficult to read (recall that ϵ_Ω and ϵ_{E_b} do not evaluate to zero for the same data points). As expected, there is better agreement for more Newtonian configurations (large $J/\mu m$) which diminishes as $J/\mu m$ decreases. There is some jaggedness at $\epsilon_\Omega = 0.0$ caused by the polynomial fitting used to estimate the minima of the EP curves. A careful examination of the apocenter data points (positive ϵ_Ω) shows that relative errors for modest values of ϵ_Ω do not exceed 20% for even the most relativ-

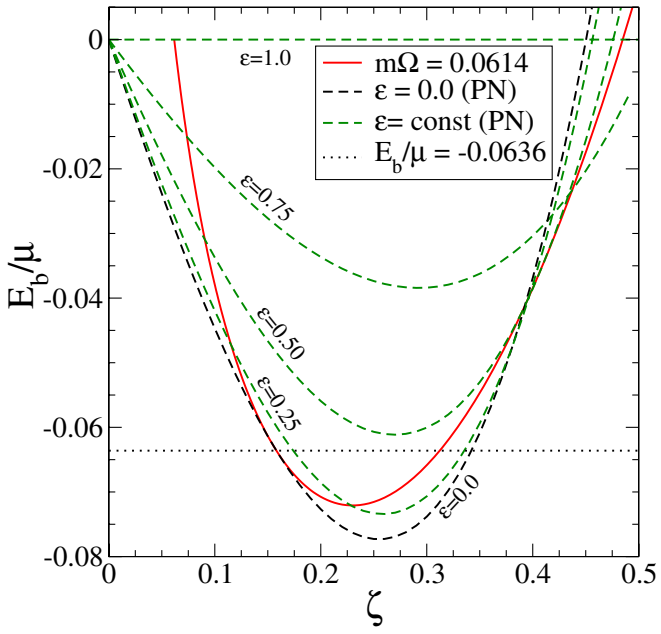

FIG. 6 (color online). Parameter space of $E(\epsilon, \zeta)$ [Eq. (9)] for nonspinning equal-mass black holes. Lines as in Fig. 5 except the horizontal dotted (black) line represents the corresponding binding energy of the numerical model.

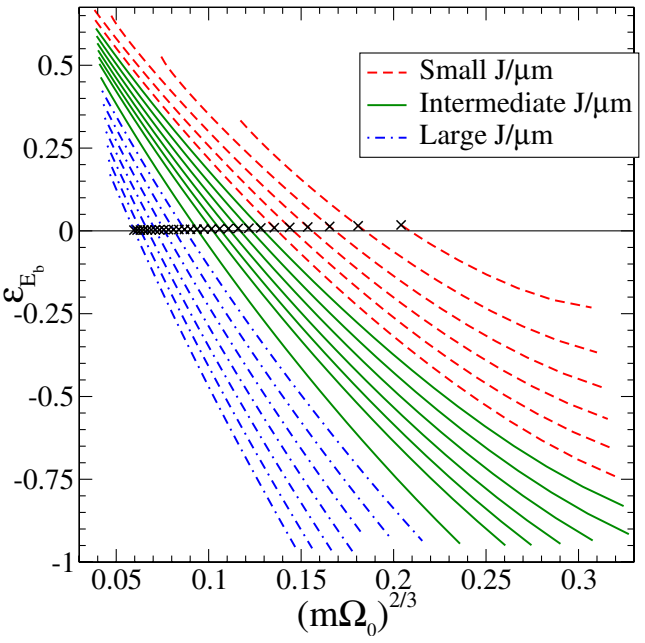

FIG. 7 (color online). Eccentricity of nonspinning equal-mass black holes computed along numerical EP curves. The 3PN ϵ_{E_b} definition of eccentricity is plotted against the orbital angular velocity. Lines are as in Fig. 3. The $\times$ symbols mark the minima of each EP curve.

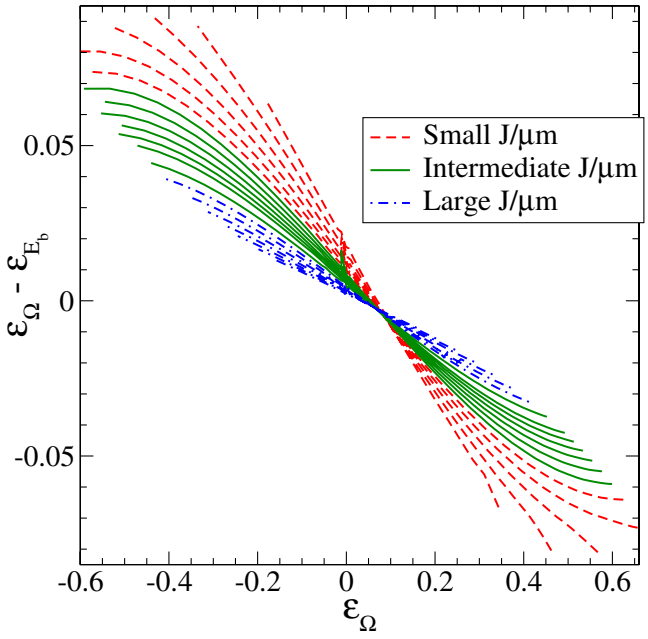

FIG. 8 (color online). Difference between ϵ_Ω and ϵ_{E_b} plotted against ϵ_Ω for nonspinning equal-mass black holes computed along numerical EP curves. Lines are as in Fig. 3.

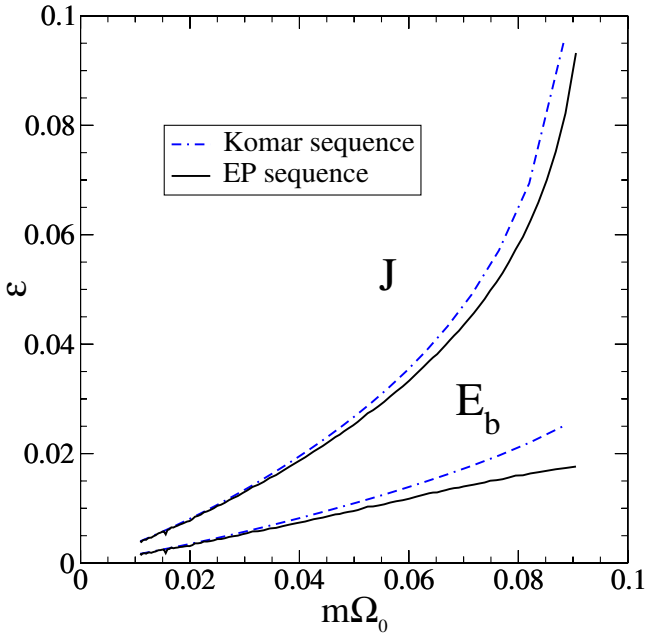

FIG. 9 (color online). The 3PN eccentricity measures ϵ_{E_b} and ϵ_J applied to both Komar and EP sequences of nonspinning equal-mass black holes. Note that the EP minima yield quasicircular data with a smaller eccentricity than is obtained from the Komar-mass ansatz.

istic cases (smallest values of $J/\mu m$). Of course, the relative errors near $\epsilon_\Omega = 0$ are unbounded. This comparison suggests that the use of either ϵ_Ω or ϵ_{E_b} yields reasonable measures for the eccentricity when applied to the numerical initial-data sets, although we should be more cautious in trusting results for pericenter data with small values of the angular momentum. Again, though, we see the uncertainty associated with any definition of eccentricity.

C. Komar-mass difference

The first application of the ϵ_{E_b} and ϵ_J definitions to nonspinning, equal-mass black-hole binary initial data was undertaken by Berti *et al.* [34]. In this work, the authors considered initial-data sets that satisfy the Komar-mass criteria for circular orbits and showed that the 3PN definitions of eccentricity ϵ_{E_b} and ϵ_J yield nonzero results for these configurations which are supposed to be in circular orbits. We reproduce these results in Fig. 9. We note that, while it is true that the circular-orbit data have nonvanishing 3PN eccentricity, the magnitude of this eccentricity smoothly approaches zero as the separation increases. We also note, as pointed out in Refs. [32,34], that the energy based definition ϵ_{E_b} yields consistently smaller values of eccentricity for the "quasicircular" data than does the angular momentum based definition ϵ_J.

In Ref. [14], we showed that circular orbits defined by the EP method yield models that are very similar to those defined by the Komar-mass ansatz. We also showed that, while very similar, all quantitative measurements of the quality of the circular orbits showed that the EP method yields better results. This is again true if we compare the 3PN eccentricities computed for nonspinning, equal-mass binaries in circular orbits defined by the EP method and the Komar-mass ansatz. The results are shown in Fig. 9, where it is clear that the EP method yields consistently smaller values of eccentricity for quasicircular orbit data.

Although the EP method yields consistently better results for circular orbits than can be obtained using the Komar-mass method, the differences are in general not sufficiently significant to outweigh the considerable computational expense associated with the EP method. When we compute eccentricities using the ϵ_Ω definition, the overhead of using the EP method is even larger. It would be useful to find another means of estimating the eccentricity of binary initial data.

In Fig. 10, we again plot the eccentricity ϵ_Ω of the same set of nonspinning, equal-mass initial data. However, on the horizontal axis, we plot the dimensionless Komar-mass difference

$$\Delta K \equiv (E_{\mathrm{ADM}} - M_{\mathrm{K}})/\mu. \tag{15}$$

We see a very strong correlation in the data, though the correlation weakens as we move farther from quasicircular orbits. It is worth noting that the EP curves with small $J/\mu m$ curve back towards zero ΔK for configurations with negative eccentricities (pericenter). This behavior is associated with data in the region of the local maxima in the EP curves. That this occurs is consistent with the notion that

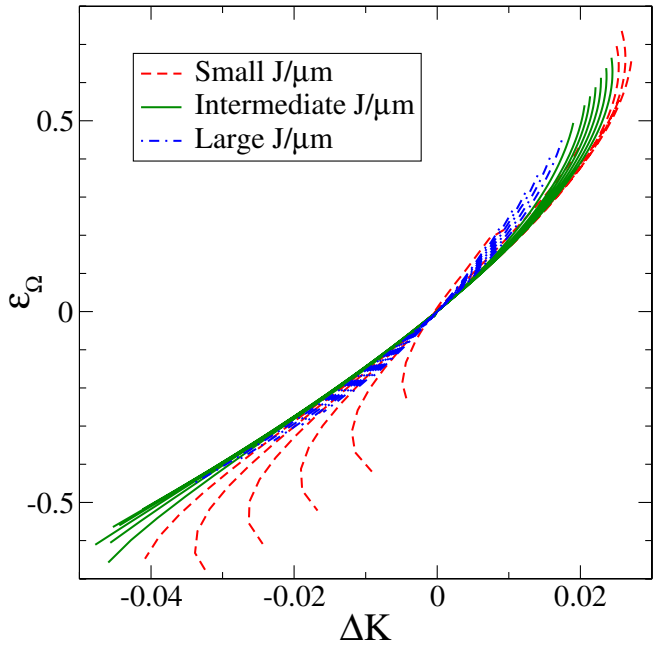

FIG. 10 (color online). The eccentricity measure ϵ_Ω applied to nonspinning equal-mass black holes computed along numerical EP curves and plotted against the Komar-mass difference ΔK. Lines are as in Fig. 3.

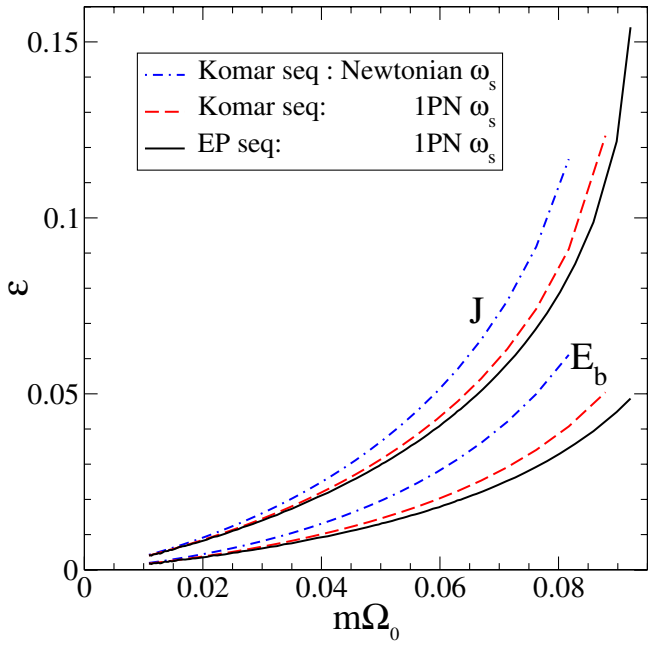

FIG. 11 (color online). The 3PN eccentricity measures ϵ_{E_b} and ϵ_J applied to both Komar and EP sequences of *corotating* equal-mass black holes. The dot-dashed (blue) lines correspond to quasicircular data defined via the Komar-mass ansatz and where the Newtonian notion of corotation is used in the 3PN equations. The dashed (red) lines show the improvement obtained by including the 1PN correction to the notion of corotation. The solid (black) lines show the added improvement of using quasicircular data based on the EP method.

these local maxima represent unstable quasicircular orbits, and hence we will find the Komar-mass difference becoming small in this region. More importantly, it shows that all of the definitions of eccentricity we have used will break down in this highly relativistic region.

V. COROTATION

So far we have restricted ourselves to the case of nonspinning black holes. However, corotating configurations have received considerable attention in spite of the fact that we do not expect to see corotating black holes in nature. In addition to the nonspinning case, Berti *et al.* [34] also computed the 3PN eccentricities for the corotating data presented in Ref. [14] and we reproduce these results in Fig. 11.

One of the primary reasons that the initial data for corotating black holes has been studied so extensively is that there is a simple and unique means of enforcing the condition of corotation on the black holes. This is in contrast to any attempt to enforce a specific value of spin (even no spin) on each black hole, which necessarily includes the uncertainty in how we define the spin of an individual black hole in a binary configuration.

The Newtonian concept of corotation implies that each black hole rotates with a spin angular velocity ω_s that is equal to the orbital angular velocity. This Newtonian notion of corotation (i.e., $\omega_s = \Omega_0$) was used by Berti *et al.* to fix the spin parameters in Eqs. (9) and (10) when using these 3PN equations to compute ϵ_{E_b} and ϵ_J. To our knowledge, this Newtonian notion of corotation has been used in *all* PN computations dealing with corotation (cf Refs. [32,34–38]). However, in Ref. [14], we have shown that there are relativistic corrections to the spin angular velocity associated with corotating black holes. We find ω_s, including the 1PN correction, to be of the form

$$\omega_s = \Omega_0(1 - \eta(m\Omega_0)^{2/3} + \cdots), \tag{16}$$

where $\eta = \mu/m$ is the symmetric mass ratio which takes the value of $1/4$ for equal-mass binaries. Also shown in Fig. 11 are two 3PN eccentricities computed using the corrected definition for ω_s. We find that using this corrected definition significantly decreases the 3PN estimated eccentricity for these circular-orbit models.

As with the nonspinning case, we can also compute the eccentricities for the corotating equal-mass binaries in quasicircular orbits defined in terms of the EP method rather than the Komar-mass ansatz. Including also the improved definition for ω_s in the 3PN definitions of eccentricity, we find the evaluated eccentricities are smallest when evaluated for quasicircular data defined by the EP method. This can also be seen in Fig. 11.

Even with the correction to ω_s, we notice the magnitude of the 3PN eccentricities computed for ''circular'' data is

consistently larger for corotating binary data than for nonspinning data. We cannot be certain why this is the case, but we should keep in mind that there is an inherent inconsistency in any attempt to attach the notion of eccentricity to corotating configurations. All of our definitions for eccentricity, including the 3PN definitions that can be evaluated using information from a single data set, ultimately rely on information from both a pericenter and an apocenter configuration. For eccentric orbits, the spins of corotating black holes will change from pericenter to apocenter. Since the spins (including spin-orbit and spin-spin couplings) contribute to the total energy, this variation of the spin throughout the orbit must impact upon our definitions of eccentricity. This is likely to cause few problems when considering nearly circular orbits (where the spin varies little from pericenter to apocenter), but our definitions of eccentricity may not yield reasonable results for orbits that deviate significantly from being circular.

VI. CONCLUSIONS

In this paper, we have examined several basic questions associated with the construction of binary black-hole initial data. When we construct data sets using the extended CTS equations and fix the freely specifiable parts of the data and boundary conditions to be consistent with the assumptions of quasiequilibrium, we obtain models for black-hole binaries in circular orbits. But if we set aside the quasiequilibrium assumption that imposes circular orbits, the resulting data can no longer evolve in a quasiequilibrium manor as the orbit will have a significant eccentricity. Our investigations suggest that the initial-data models we obtain represent, in general, binaries that are at *turning points* (either apocenter or pericenter) of some general eccentric orbit.

The specific notion of quasiequilibrium that we set aside is implemented by imposing either the Komar-mass condition or by choosing the minimum of an EP curve as our circular-orbit model. If, as it seems, general initial-data models on an EP curve are at turning points, then we can use information from these models to estimate the eccentricity of the model's orbits. Of course, there is no unique definition of eccentricity. We have examined several possible definitions for eccentricity. Using only information from the initial-data sets on an EP curve, we have defined two eccentricities for an orbit (ϵ_Ω and ϵ_d), but these definitions require that we have representative models at both the pericenter and apocenter turning points of a given orbit (assumed to have constant binding energy). We have compared these definitions of eccentricity to the 3PN definitions (ϵ_{E_b} and ϵ_J) developed by Mora and Will [32]. All of the definitions agree quite well for nonrelativistic orbits. They are also in reasonably good agreement for more tightly bound and relativistic orbits as well, although the results are quantitatively different. One might ask which definition is better for more relativistic situations. However, it is not clear that there is a meaningful answer.

In comparing the numerical and 3PN eccentricity measures for relativistic cases, we have noticed an interesting and initially unexpected feature of the 3PN equations. Figure 2 compares numerical and 3PN EP curves for equal-mass nonspinning black-hole binaries. The EP curves each have a constant value for the orbital angular momentum. All of the numerical EP curves cover a finite range of separations (parametrized by $m\Omega_0$). This is because it becomes computationally expensive to compute models at very large separations (small $m\Omega_0$) and it becomes increasingly difficult to obtain convergent solutions at very small separations. What was initially unexpected is that some of the 3PN EP curves also cover a finite range of separations.

For sufficiently small values of $J/\mu m$, the 3PN EP curves do not extend to configurations with arbitrarily large separation. To make this clear, Fig. 2 includes a curve that marks the boundary (for both large and small separation) of the 3PN EP curves. This is most easily seen for the 3PN EP curves near the bottom of Fig. 2. Here we can see that the 3PN EP curves do not extend to arbitrarily small values of $m\Omega_0$, but the numerical EP curves do (although we do not compute them for arbitrarily large separation).

That this behavior is not an artifact of our method for computing the 3PN EP curves can be seen by examining Fig. 5. Recall that angular momentum is held constant along EP curves, so an EP curve is represented by a horizontal line in this figure. Notice that all curves of constant eccentricity have a local minimum. For $J/\mu m \gtrsim 3.4$, an EP curve can extend from $\epsilon = 0 \rightarrow 1$. However, for $J/\mu m \lesssim 3.4$, an EP curve can only extend from $\epsilon = 0$ to a maximum eccentricity that is less than 1, and is determined by which curve of constant ϵ has its minimum tangent to the EP curve.

This behavior in the 3PN EP curves is clearly related to the fact that, for sufficiently small values of $J/\mu m$, the EP curves each have a local maximum at small separation. In spite of the fact that ϵ_{E_b} and ϵ_J can be evaluated using data from a single model, the parametrization of the 3PN energy and angular momentum in terms of eccentricity and semilatus rectum used by Mora and Will [32] is, at its heart, based on a ''two-point'' method. Neither the numerical nor PN approaches should be able to define an eccentricity for a point on the EP curve with an energy larger than that at the local maximum at small separation. Unfortunately, this does not explain all of the unusual behavior seen in these 3PN EP curves as we note that in Fig. 2 the 3PN EP curves for small $J/\mu m$ extend to separations *smaller* than the location of the local maximum. What is clear is that this behavior is an artifact of the parametrization of the 3PN equation in terms of the eccentricity and semilatus rectum. The original 3PN equation, parametrized in terms of, for example, separation and tangential velocity, do not have

any problem in constructing EP curves that extend to infinite separation.

Given the strong correlation between the various measures of eccentricity and the difference between the Komar mass and the ADM energy as measured by ΔK and seen in Fig. 10, we suggest that perhaps ΔK can serve as a useful invariant means of parametrizing the eccentricity of an orbit. However, initial-data studies can at best suggest possible useful parametrizations. It will be most useful to evolve initial data that are significantly eccentric and examine the orbital dynamics to better understand both the parametrization of eccentricity and its effects on the dynamics. For example, it may be particularly interesting to explore the evolution of eccentric initial data for an ''orbit'' that has no pericenter turning point on its EP curve.

ACKNOWLEDGMENTS

We would like to thank Harald Pfeiffer, Alessandra Buonanno, Clifford Will, and Emanuel Berti for useful discussions. This work was supported by NSF Grant No. PHY-0555617 to Wake Forest University. G. C. acknowledges support from the Z. Smith Reynolds Foundation. Computations were performed on the Wake Forest University DEAC Cluster with support from an IBM SUR grant and the Wake Forest University IS Department.

[1] M. Boyle, D. A. Brown, L. E. Kidder, A. H. Mroué, H. P. Pfeiffer, M. A. Scheel, G. B. Cook, and S. A. Teukolsky, Phys. Rev. D **76**, 124038 (2007).
[2] F. Pretorius, Phys. Rev. Lett. **95**, 121101 (2005).
[3] M. Campanelli, C. O. Lousto, P. Marronetti, and Y. Zlochower, Phys. Rev. Lett. **96**, 111101 (2006).
[4] J. G. Baker, J. Centrella, D. Il Choi, M. Koppitz, and J. van Meter, Phys. Rev. Lett. **96**, 111102 (2006).
[5] P. Diener, F. Herrmann, D. Pollney, E. Schnetter, E. Seidel, R. Takahashi, J. Thornburg, and J. Ventrella, Phys. Rev. Lett. **96**, 121101 (2006).
[6] M. A. Scheel, H. P. Pfeiffer, L. Lindblom, L. E. Kidder, O. Rinne, and S. A. Teukolsky, Phys. Rev. D **74**, 104006 (2006).
[7] B. Brügmann, J. A. Gonzalez, M. Hannam, S. Husa, U. Sperhake, and W. Tichy, Phys. Rev. D **77**, 024027 (2008).
[8] M. Marronetti, W. Tichy, B. Brügmann, J. A. Gonzalez, M. Hannam, S. Husa, and U. Sperhake, Classical Quantum Gravity **24**, S43 (2007).
[9] F. Herrmann, I. Hinder, D. Shoemaker, and P. Laguna, Classical Quantum Gravity **24**, S33 (2007).
[10] Z. B. Etienne, J. A. Faber, Y. T. Liu, S. L. Shapiro, and T. W. Baumgarte, Phys. Rev. D **76**, 101503 (2007).
[11] P. C. Peters, Phys. Rev. **136**, B1224 (1964).
[12] G. B. Cook, Phys. Rev. D **50**, 5025 (1994).
[13] E. Gourgoulhon, P. Grandclément, and S. Bonazzola, Phys. Rev. D **65**, 044020 (2002).
[14] M. Caudill, G. B. Cook, J. D. Grigsby, and H. P. Pfeiffer, Phys. Rev. D **74**, 064011 (2006).
[15] M. L. Skoge and T. W. Baumgarte, Phys. Rev. D **66**, 107501 (2002).
[16] G. B. Cook, M. W. Choptuik, M. R. Dubal, S. Klasky, R. A. Matzner, and S. R. Oliveira, Phys. Rev. D **47**, 1471 (1993).
[17] S. Brandt and B. Brügmann, Phys. Rev. Lett. **78**, 3606 (1997).
[18] T. Damour, P. Jaranowski, and G. Schaefer, Phys. Rev. D **62**, 044024 (2000).
[19] G. B. Cook and H. P. Pfeiffer, Phys. Rev. D **70**, 104016 (2004).
[20] J. W. York, Jr., Phys. Rev. Lett. **82**, 1350 (1999).
[21] H. P. Pfeiffer and J. W. York, Jr., Phys. Rev. D **67**, 044022 (2003).
[22] G. B. Cook, Phys. Rev. D **65**, 084003 (2002).
[23] A. Ashtekar and B. Krishnan, Phys. Rev. D **68**, 104030 (2003).
[24] A. Ashtekar, C. Beetle, O. Dreyer, S. Fairhurst, B. Krishnan, J. Lewandowski, and J. Wiśniewski, Phys. Rev. Lett. **85**, 3564 (2000).
[25] J. L. Jaramillo, E. Gourgoulhon, and G. A. M. Marugán, Phys. Rev. D **70**, 124036 (2004).
[26] T. W. Baumgarte, Phys. Rev. D **62**, 024018 (2000).
[27] H. P. Pfeiffer, S. A. Teukolsky, and G. B. Cook, Phys. Rev. D **62**, 104018 (2000).
[28] D. Christodoulou, Phys. Rev. Lett. **25**, 1596 (1970).
[29] L. B. Szabados, Living Rev. Relativity **7**, 4 (2004), http://www.livingreviews.org/lrr-2004-4.
[30] B. Krishnan, C. O. Lousto, and Y. Zlochower, Phys. Rev. D **76**, 081501(R) (2007).
[31] R.-M. Memmesheimer, A. Gopakumar, and G. Schäfer, Phys. Rev. D **70**, 104011 (2004).
[32] T. Mora and C. M. Will, Phys. Rev. D **69**, 104021 (2004).
[33] T. Mora and C. M. Will, Phys. Rev. D **66**, 101501(R) (2002).
[34] E. Berti, S. Iyer, and C. M. Will, Phys. Rev. D **74**, 061503(R) (2006).
[35] T. Damour, E. Gourgoulhon, and P. Grandclément, Phys. Rev. D **66**, 024007 (2002).
[36] L. Blanchet, Phys. Rev. D **65**, 124009 (2002).
[37] L. Blanchet, in *2001: A Relativistic Spacetime Odyssey*, edited by I. Ciufolini, D. Dominici, and L. Lusanna (World Scientific, River Edge, NJ, 2003), p. 411.
[38] M. Campanelli, C. O. Lousto, and Y. Zlochower, Phys. Rev. D **74**, 084023 (2006).